Journal of Nuclear Materials 417 (2011) 508–511
DOI:http://dx.doi.org/10.1016/j.jnucmat.2011.01.077

La_2O_3-reinforced W and W–V alloys produced by hot isostatic pressing

A. Muñoz [a,*], M.A. Monge [a], B. Savoini [a], M.E. Rabanal [b], G. Garces [c], R. Pareja [a]

[a] Departamento de Física, Universidad Carlos III de Madrid, 28911 Leganés, Spain
[b] Departamento de Ciencia e Ingenieria de Materiales e Ingenieria Quimica, Universidad Carlos III de Madrid, 28911 Leganés, Spain [c] Centro Nacional de Investigaciones Melatúrgicas, CENIM, 28040 Madrid, Spain

Abstract: W and W V alloys reinforced with La_2O_3 particles have been produced by MA and subsequent HIP at 1573 K and 195 MPa. The microstructure of the consolidated alloys has been characterized by scanning electron microscopy, energy dispersive spectroscopy analyses and X ray diffraction. The mechanical properties were studied by nanoindentation measurements. The results show that practically full dense billets of W V, W V La_2O_3 and W La_2O_3 alloys can be produced. The microstructure analysis has shown that islands of V are present in W V and W V $1La_2O_3$ alloys. In W $1La_2O_3$ islands of La_2O_3 are also pres ent. The nanohardness of the W matrix increases with the addition of V, while decreases with the addi tion of La_2O_3.

1. Introduction

W is a principal candidate materials for fabricating plasma facing components (PFC) in a future fusion power reactor due to its high melting temperature, good thermal conductivity, thermal stress resistance, low tritium retention and high temperature strength [1,2]. For these applications, the structural materials should have an operating temperature window 873 1600 K and a ductile brittle transition temperature (DBTT) in the interval 573 673 K, as well as a recrystallization temperature (RT) above 1600 K [3 5]. L a $_2O_3$ dispersion or Al K Si doping can improve the mechanical strength and increase the tungsten RT, although the DBTT appears not to be lowered [6,5]. Most of these W alloys were prepared by powder metallurgy methods, in particular by ball milling and subsequent pressure less sintering or hot isostatic pressing (HIP) [7 11]. Recently, W and W Ti alloys reinforced with Y_2O_3 have been sintered by HIP [12]. The use of Ti as sintering acti vator and the Y_2O_3 dispersion result in full dense materials exhib iting improved mechanical properties and oxidation resistance [13]. However, the Y_2O_3 particles in a W matrix appear to be unsta ble at temperatures above $\sim$1600 K becoming into coarse particles of complex W Y and W Y Ti oxides, which could worsen the mechanical properties. This drawback may be avoided if V is used as sintering activator. The V W system exhibits an isomorphous phase diagram with a continuous range of solid solution [14].

The aim of the present work is to produce W and W V alloys rein forced with La_2O_3 particles and investigate their microstructure and thermal stability in order to obtain a structural material with favor able properties to be used for developing PFC.

2. Experimental

The starting materials were 99.9% pure W and 99.5% pure V powders with an average particle size of 14 and 20 μm, respec tively, and 99.9% pure nanometric La_2O_3 powder with particle sizes between 10 and 30 nm. Powder blends with the target composi tions in weight: W 1%La_2O_3, W 4%V, W 2%V and W 4%V 1%La_2O_3 were prepared mixing together the powders for 4 h in a mixer. The powder blends were mechanically alloyed (MA), inside a WC vessels sealed under a high purity Ar atmosphere, for 10 h in a high energy planetary mill. WC balls of ∅ 10 mm were used as grinding media with a ball powder ratio of 4:3. Afterwards, the alloyed powders were canned and degassed at 673 K for 24 h in vacuum and then the cans were vacuum sealed. The starting pow ders, as well as the blends and alloyed powders were manipulated under a high purity Ar atmosphere using a glove box. The alloyed powder inside the cans was HIP treated at 1573 K for 2 h at a pressure of 195 MPa.

The compositions of the consolidated alloys, along with their densities measured using a He ultrapycnometer, are given in Table 1. The microstructural characteristics of the materials were investigated using light microscopy, scanning electron microscopy (SEM) and energy dispersive spectroscopy (EDS) analyses. More over, X ray diffraction (XRD) analyses were made by the Rietveld method using the Fullprof program [15]. The average crystallite size of the milled powders was determined from the diffraction peak widths taking into account the of diffractometer resolution function. The thermal behavior of the alloyed powders in the range

* Corresponding author. Tel.: +34 916249413; fax: +34 916248749.
E-mail addresses: angel.munoz@uc3m.es (A. Muñoz), mmonge@fis.uc3m.es (M.A. Monge), bsavoi@fis.uc3m.es (B. Savoini), eugenia@ing.uc3m.es (M.E. Rabanal), ggarces@cenim.csic.es (G. Garces), rpp@fis.uc3m.es (R. Pareja).

Table 1
Lattice parameters after each stage of the powder processing and density of the consolidated alloys.

	Blended	Milled		HIP treated		
	a (nm)	*a* (nm)	Crystallite size (nm)	*a* (nm)	Density	
					Theor. (g/cm^3)	Relat. (%)
W–1La_2O_3	–	0.3167	116	0.3167	18.9	90.6
W–2V	W: 0.3166V: 0.3035	0.3171	26	0.3164	18.5	95.6
W–4V	W: 0.3170V: 0.3038	0.3165	49	0.3159	17.7	98.1
W–4V–1La_2O_3	W: 0.3167V: 0.3033	0.3167	130	0.3160	17.3	97.7

500 1873 K was investigated by differential thermal analysis (DTA) at a heating rate of 10 K/min in flowing pure Ar. Nanoinden tation tests at room temperature using a Berkovich indenter were carried out in a Nanoindenter XP. The maximum penetration depth was 300 nm.

3. Results and discussion

3.1. Powder characterization

Fig. 1 shows the milling effect on the diffraction pattern of the investigated powder blends. Only for the blended W 4V powder, the diffraction peaks corresponding to pure W and pure V are separated. After milling the XRD pattern for W 4V exhibited a single bcc phase, suggesting that part of the V content is dis solved in the W lattice. However, the expected reduction in the lattice parameter for such solid solution was not observed (Table 1). It could occur that milling only refine the V particles and disperse them more homogenously. Then, the weak intensity of the XRD beams from the refined V particle, and a strong absorption of these beams by the W particles, can explain the ab sence of V diffraction peaks. In spite of this, it should be noted that the milling originates a high level of internal stresses in the W grains. This can also affect the lattice parameter and coun terbalance the decrease attributable to the V dissolution in W. Thus, other type of measurements are required to elucidate if milling under the present condition results in a complete or par tial V dissolution in W. Similar results were obtained for W 2V and W 4V 1La_2O_3. For milled W 4V, a weak (1 1 0) reflection attributable to V was detected. WC or W_2C impurities coming from the grinding media were not detected in the patterns. Ta ble 1 shows the average crystallite size in the milled powders. The average crystallite size increased significantly adding 1%La_2O_3 or increasing the V fraction.

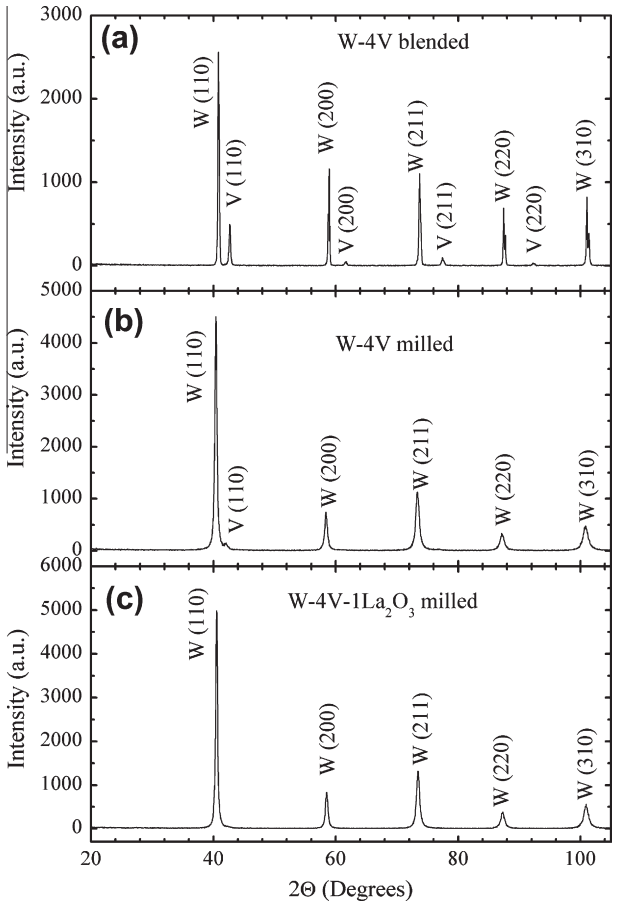

Fig. 1. Effect of 10 h milling on the XRD patterns for W–V powders. (a) Blended W–4V, (b) milled W–4V, and (c) milled W–4V–1La_2O_3.

Fig. 2 shows SEM images from back scattered electrons (EBS) for the blended and milled powders. After milling, the BSE images can not discriminate the two initial metallic phases showing a rather uniform contrast, which suggests certain homogeneity in the com position of the powder. Also, the powder refinement is evident. Evidence for La_2O_3 agglomeration was not observed. Similar results were obtained for the other alloys.

The DTA curves of the milled powders are shown in Fig. 3. On heating, a very broad exothermic peak centered at ~873 K is ob served. It is attributed to recovery of the lattice defects induced by milling. The continuous exothermal reaction starting at ~1473 K for pure W and W 1La_2O_3 would correspond to the so lid state sintering. Addition of V decreases the sintering onset to ~1223 K, indicating that V is a solid state sintering activator for W.

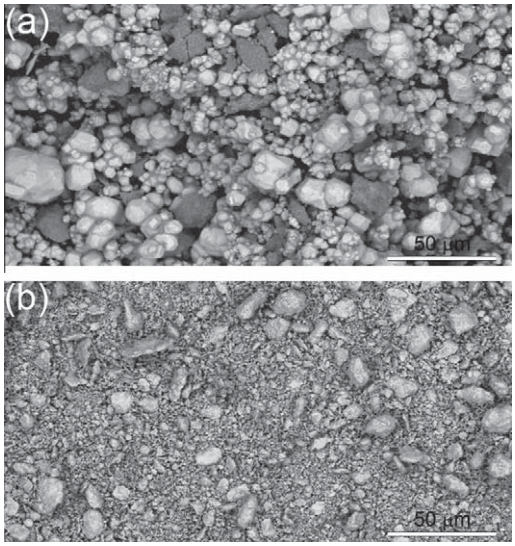

Fig. 2. BSE images for W–4V–1La_2O_3. (a) Blended for 4 h, and (b) milled for 10 h.

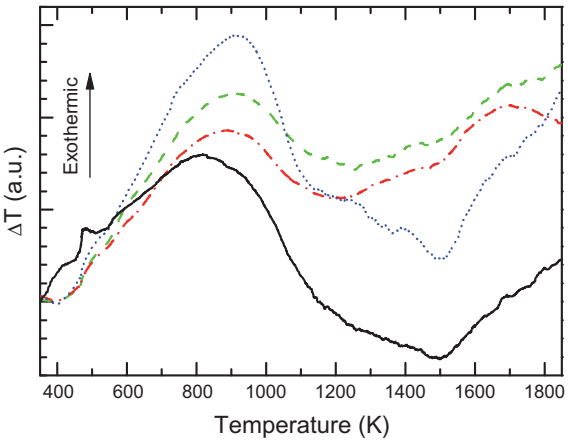

Fig. 3. Effect of V and La_2O_3 additions on the DTA curves for mechanical alloyed W powders: W (solid line), W–4V (dashed), W–1La_2O_3 (dot) and W–4V–1La_2O_3 (dash dot).

3.2. Microstructure of the consolidated alloys

3.2.1. W 1La_2O_3

The microstructure of W 1La_2O_3 is shown in Fig. 4. The element map images revealed the presence of La_2O_3 and small pores (Fig. 4c) uniformly distributed in the material. The irregular shapes of the pores and oxide pools suggest that solid state sintering of W 1La_2O_3 is not completely accomplished under the present HIP conditions.

3.2.2. W V

Addition of V to W favored HIP sintering as the density measurements and SEM observations revealed. Fig. 5 shows the microstructure and element map image for sintered W 4V. Besides fine V pools uniformly distributed, the V element map image (Fig. 5b) indicates that V is also present in the W matrix. Since W and V are miscibile each other, the presence of V pools indicates that a part of V particles were not dissolved in the milling process. In any case, the milling process favors the formation of a homogenous and fine dispersion of V in the sintered W V material.

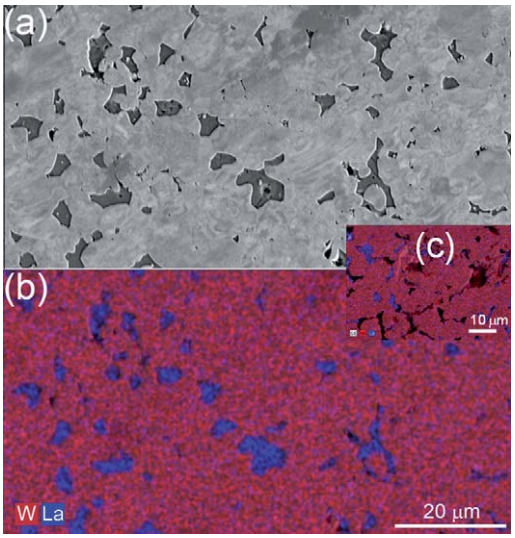

Fig. 4. Microstructure of HIP sintered W–1La_2O_3. (a) BSE image, (b) element map image showing the La and W distributions, and (c) element map image showing the presence of small pores (black areas).

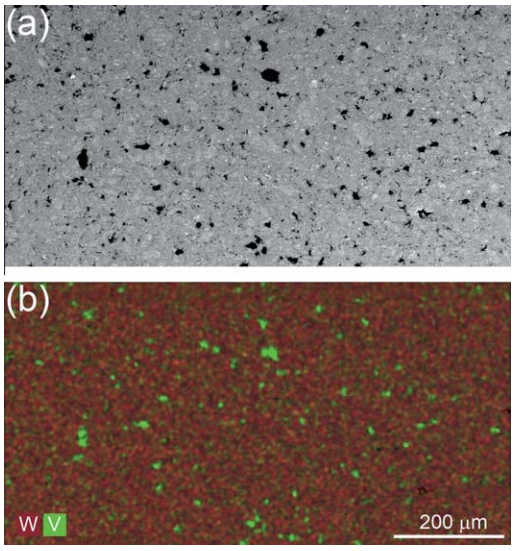

Fig. 5. Microstructure of HIP sintered W–4V. (a) BSE image and (b) element map image for the V and W distributions.

3.2.3. W 4V 1La_2O_3

Addition of 1%La_2O_3 to W V alloys enhanced the V dispersion in W a s Fig. 6 shows for W 4V 1La_2O_3. Moreover, it is worthwhile to notice that presence of V in the alloy inhibited the La_2O_3 agglomeration promoting the fine dispersion of La in the alloy induced as the corresponding element map images in Figs. 4 6 reveal. In addition, Fig. 6c reveals that much less La is present in the V pools than in the W matrix.

In the XRD measurements performed on the W V and W 4V 1La_2O_3 samples only the diffraction peaks of a single bcc phase are observed even though the SEM images revealed the presence of a second V phase, which fraction might not to be high enough to be detected by XRD. Nevertheless, the measured lattice parameter for W 4V is significantly smaller than the one for W 2V (Table 1) indicating that V fraction in solid solution is higher in W 4V.

3.3. Mechanical measurements

Fig. 7 shows the nanohardness value and the elastic modulus as a function of the penetration depth for selected nanoindentations

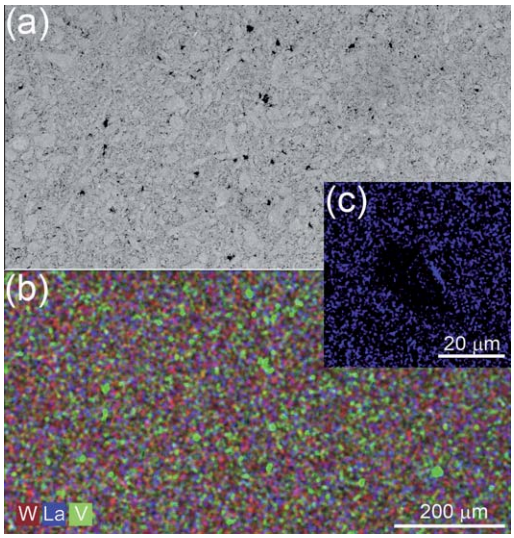

Fig. 6. Microstructure of HIP sintered W–4V–La_2O_3. (a) BSE image, (b) element map images for V, W and La, and (c) element map image showing the La distribution around a V pool.

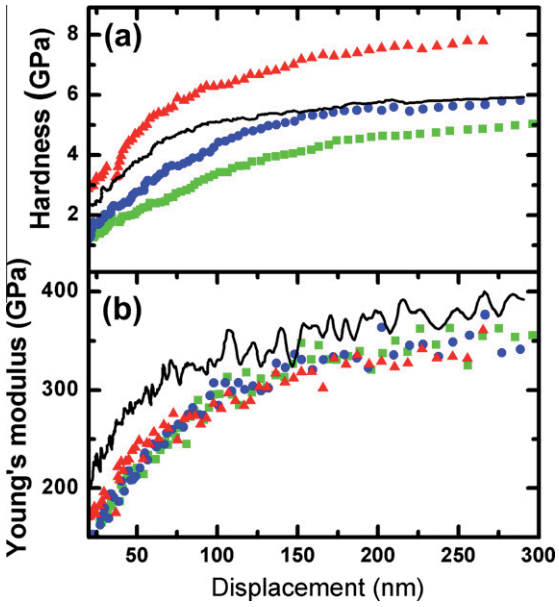

Fig. 7. (a) Nanohardness and (b) Young's modulus, as a function of the indentation depth for HIP sintered W alloys: W–4V–1La_2O_3 (solid line), W–2V (circles), W–4V (triangles), and W–1La_2O_3 (squares).

within the W matrix. These results show that the V addition increases nanohardnes and La_2O_3 lowers it. Indentations performed on the interparticle V phase of the W V alloys exhibited a much higher nanohardnes values than those in the W matrix, although these values presented a high dispersion. These results are attributed to the differences in composition and/or to the high stress concentration in these interparticle phases, as it was suggested by the microstructural analyses. The elastic modulus for W 4V 1La_2O_3 results in 400 GPa in very good agreement to the reported values for pure W. However, values a rather lower, i.e. ~350 GPa, were measured for the W V and W 1La_2O_3 alloys.

4. Conclusions

Practically full dense billets of W V, W V La_2O_3 and W La_2O_3 alloys can be produced by mechanical alloying and subsequent HIP sintering at 1573 K and 195 MPa. The microstructure analyses of the consolidated alloys have shown the presence of V pools in the W V and W V La_2O_3 alloys. This suggests that the present milling conditions did not promote the perfect dissolution of V in W for the concentrations studied, apparently. In W La_2O_3 pools of La oxide are observed. However, the concurrent addition of V and La_2O_3 inhibited the formation of these pools promoting the dispersion or dissolution of La and V in the W matrix. The nanoindentation measurements have shown that the addition of V increases nanohardness and the presence of La_2O_3 lowers it.

Acknowledgments

This investigation was supported by the EURATOM/CIEMAT association (deliverable EFDA WP08 09 MAT WWALLOY), the Comunidad de Madrid (ESTRUMAT CM S0505/MAT/0077) and the Spanish Ministry of Science and Innovation (ENE2008 06403 C06 04).

References

[1] V. Barabash, M. Akiba, I. Mazul, M. Ulrickson, G. Vieider, J. Nucl. Mater. 233–237 (1996) 718–723.
[2] I. Smid, M. Akiba, G. Veider, L. Plöchl, J. Nucl. Mater. 258–263 (1998) 160–172.
[3] P. Norajitra, L.V. Boccaccini, E. Diegele, et al., J. Nucl. Mater. 329–333 (2004) 1594.
[4] H. Bolt, V. Barabash, W. Krauss, J. Linke, R. Neu, S. Suzuki, N. Yoshida, Asdex Upgrade Team, J. Nucl. Mater. 329–333 (2004) 66.
[5] M. Rieth, B. Dafferner, J. Nucl. Mater. 342 (2005) 20.
[6] M. Faleschini, H. Kreuzer, D. Kiener, R. Pippan, J. Nucl. Mater. 367–370 (2007) 800.
[7] M.N. Avvetand-Fènoël, R. Taillard, J. Dhers, J. Foct, Int. J. Refract. Hard Mater. 21 (2003) 205–213.
[8] H.J. Ryu, S.H. Hong, Mater. Sci. Eng. A 363 (2003) 179–184.
[9] Y. Chen, Y.C. Wu, F.W. Yur, J.L. Chen, Int. J. Refract. Hard Mater. 26 (2008) 525–529.
[10] S. Saito, K. Fukaya, S. Ishiyama, K. Sato, J. Nucl. Mater. 307–311 (2002) 1542–1546.
[11] Y. Ishijima, H. Kurishita, K. Yubuta, H. Arakawa, M. Hasegawa, Y. Hiraoka, T. Takida, K. Takebe, J. Nucl. Mater. 329–333 (2004) 775–779.
[12] M.A. Monge, M.A. Auger, T. Leguey, Y. Ortega, L. Bolzoni, E. Gordo, R. Pareja, J. Nucl. Mater. 386–388 (2009) 613.
[13] M.V. Aguirre, A. Martín, J.Y. Pastor, J. LLorca, M.A. Monge, R. Pareja, Metall. Mater. Trans. 40A (2009) 2283–2290.
[14] S.V. Nagender Naidu, A.M. Sriramamurthy, M. Vijayakumar, P. Rama Rao, in: J.F. Smith (Ed.), Phase Diagrams of Vanadium Alloys, Monograph Series on Alloy Phase Diagrams, ASM International, Metal Parks, Ohio, 1989, p. 313.
[15] J. Rodríguez-Carvajal, Physica B 192 (1993) 55.